17

Fundamentals of Airborne Acoustic Positioning Systems

Fernando J. Álvarez Franco

SENSORY SYSTEMS RESEARCH GROUP, UNIVERSITY OF EXTREMADURA, BADAJOZ, SPAIN

1 Introduction

Active acoustics has been extensively used in the design of airborne local positioning systems for the last two decades, and it is today considered a classical and reliable solution to this technological challenge (Mautz, 2012). Using typical working frequencies within the high sonic and very low ultrasonic bands (15,000–50,000 Hz), this solution is characterized by a centimeter precision with coverage ranges of some tens of meters.

Although acoustics had been already used to locate and track submerged objects since the early 1960s (Milne, 1983), it is not after more than thirty years that the first airborne acoustic positioning systems (AAPS) were developed. These pioneering systems were based on the emission of short and constant-frequency ultrasonic pulses whose arrival was detected by following a simple amplitude or energy thresholding procedure. This was, for example, the case of the Active Bat System (Ward et al., 1997) where wireless badges (bats) carried by personnel or attached to certain equipment emitted 40-kHz ultrasonic pulses of 50 μs-duration after being triggered over a wireless link. These pulses were received by a set of ceiling-mounted sensors that measured the pulses Time-of-Arrival (TOA) and computed the badge three-dimensional position by spherical lateration. An alternative approach was proposed in the Constellation System (Foxlin and Harrington, 1998), where a set of ultrasonic emitters was deployed at known locations in the environment. These beacons emitted a 40-kHz ultrasonic pulse after receiving an infrared trigger code from the unit to be located, which communicated with the beacons one-at-a-time. The receiving unit needed to compute at least three TOAs from the emissions of different beacons to obtain its position by spherical lateration. Note that, in this case, the device to be located was in charge of computing its own position using the signals emitted from different beacons. This architecture has been defined by some authors as privacy-oriented, in contrast to the centralized architecture of the Active Bat system. An additional example of a narrowband AAPS that cannot be considered centralized or privacy-oriented is the Cricket system (Priyantha et al., 2000). This system was based on a set of independent beacons

Geographical and Fingerprinting Data for Positioning and Navigation Systems. https://doi.org/10.1016/B978-0-12-813189-3.00017-4

that incorporated an RF transceiver, an ultrasonic emitter, and an ultrasonic receiver. Each beacon could compute its own position by measuring the TOAs of the 40-kHz ultrasonic pulses of 125 μs-duration emitted by nearby beacons, which also broadcast their own position through a 433-MHz RF signal. Again, spherical lateration was used to compute the desired location. All these systems featured very simple emitter and receiver acoustic modules, but at the expense of providing a limited positioning accuracy of some decimeters with high sensitivity to in-band noise. Moreover, special attention had to be paid to avoid interference between different emitters, either by making use of time-multiplexing strategies (Foxlin and Harrington, 1998) by developing specific algorithms (Priyantha et al., 2000).

A solution to these limitations was soon provided by the pulse compression technique extensively used in radar systems (Skolnik, 1980). A new generation of broadband AAPS started being developed in the early 2000s, based on the emission of Binary Phase Coded signals that, as will be detailed later, were detected by matched filtering. This spread spectrum technique had been successfully incorporated in the development of high precision airborne sonars some years before (Peremans et al., 1993; Jörg and Berg, 1998; Ureña et al., 1999), so its application in the field of AAPS was rather straightforward. One of the first broadband AAPS is presented in Hazas and Ward (2002, 2003), where the authors propose the use of 511-bit Gold codes to modulate a 50-kHz ultrasonic carrier with a bit period of 50 μs, thus giving a total emission duration of 25.55 ms. In Hazas and Ward (2002), eight receivers are installed in the ceiling of an office room to configure a centralized architecture that measures the TOAs of the signals emitted by a set of synchronized transmitters. The authors reported positioning accuracies slightly above 2 cm when using spherical lateration in a noisy environment. In Hazas and Ward (2003), a privacy-oriented architecture is presented with positioning accuracies around 5 cm. A similar privacy-oriented architecture is presented in Villadangos et al. (2005), based on the modulation of a 50-kHz carrier with 127-bit Gold codes and a bit period of 20 μs, for a significantly shorter emission duration of 2.54 ms. The main contribution of this broadband AAPS is the proposal of a hyperbolic lateration algorithm, based on the measurement of the Time-Difference-of-Arrival (TDOA) between the first detected signal, emitted by the nearest beacon, and the other signals detected subsequently. This positioning strategy avoids the need for a synchronized triggering signal between the beacons and the receiver. An improved version of this system is presented in Ureña et al. (2007), where the 50 kHz carrier is modulated by 255-bit Kasami codes to obtain accuracies below 1 cm in the horizontal positioning of the receiver. Since the appearance of these initial works, other pseudo-random sequences have been proposed to encode the emissions of more computationally efficient broadband AAPS, such as LS (Pérez et al., 2007) or CSS (Pérez et al., 2012). In all these broadband systems, the TOA or TDOA of the received signal is measured when the auto-correlation peak of this signal exceeds a detection threshold, what improves the precision of the range measurement between one and two orders of magnitude with respect to that of the previous narrowband systems. Nevertheless, the longer duration of AAPS signals leads to the appearance of new problems that may hinder their detection.

Some of the most recent works in the field of broadband AAPS are focused on the proposal of solutions to compensate for some of these problems, such as Doppler shift (Álvarez et al., 2013), multipath propagation (Álvarez et al., 2017a), or Multiple Access Interference (MAI) (Aguilera et al., 2018b).

This chapter has been written to give the reader a general overview of AAPS design fundamentals. With this idea in mind, next section includes some basic concepts and results related with acoustic wave propagation in air, which eventually determine the limits of this technology performance. Next, Section 3 deals with the signal detection process and describes the different positioning observables. Section 4 reviews those positioning strategies directly related with the most used observables described in the previous section. Finally, the above mentioned signal detection hindering phenomena and compensation techniques are described in some detail in Section 5.

2 Acoustic Wave Propagation in Air

As stated before, the performance of acoustic technology is directly related to the propagation characteristics of these waves in air. Some of these characteristics are briefly reviewed next.

2.1 Absorption

Acoustic waves are longitudinal mechanical waves that propagate through a material medium by pressure variations. When they propagate, part of the energy is dissipated as heat inside the medium, thus causing an exponential decay or the pressure amplitude P with the traveled distance r as,

$$P(r) \propto e^{-\alpha \cdot r}, \tag{1}$$

where α is the absorption coefficient. In the air, there are basically two different mechanisms that cause absorption of acoustic waves: the viscothermal losses (or classical absorption) and the oxygen and nitrogen molecular relaxation processes. The theoretical analysis of both processes led to a set of equations that have been later experimentally adjusted to increase agreement with real data. Today, these equations are grouped into the ISO-9613 standard (ISO/TC 43 Technical Committee, Acoustics, Sub-Committee SC1, Noise, 1993). This norm establishes that the absorption coefficient can be calculated as,

$$\begin{aligned}\alpha(\mathrm{dB/m}) = 8.69 f^2 \Bigg\{ & 1.84 \cdot 10^{-11} \left(\frac{P}{P_{ref}}\right)^{-1} \cdot \left(\frac{T}{T_{ref}}\right)^{\frac{1}{2}} \\ & + \left(\frac{T}{T_{ref}}\right)^{\frac{-5}{2}} \cdot \left[0.01275 \frac{e^{\frac{-2239.1}{T}}}{f_{rO} + \frac{f^2}{f_{rO}}} + 0.1068 \frac{e^{\frac{-3352}{T}}}{f_{rN} + \frac{f^2}{f_{rN}}} \right] \Bigg\},\end{aligned} \tag{2}$$

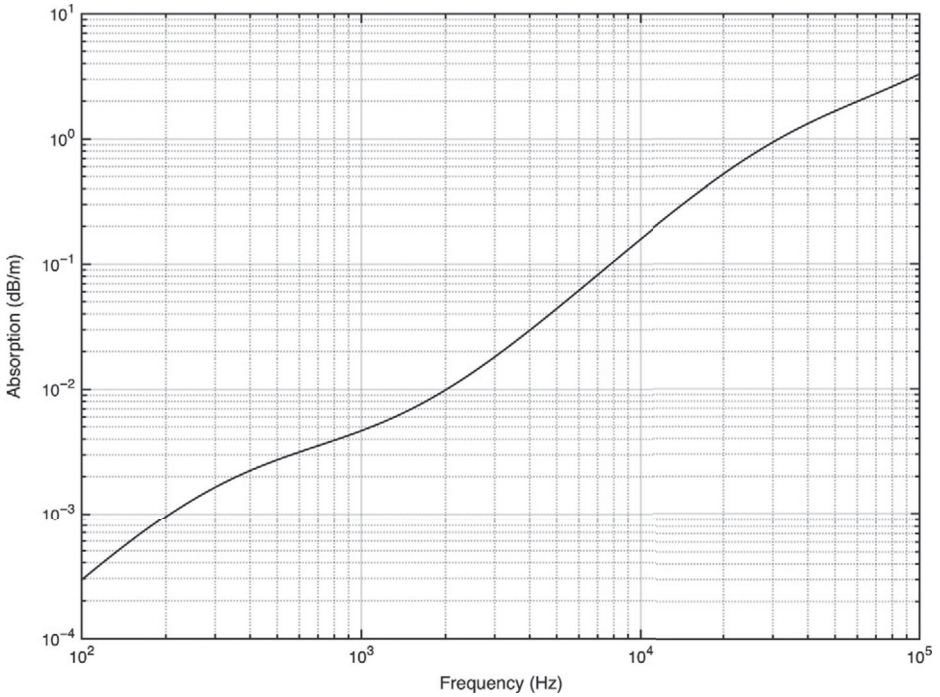

FIG. 1 Frequency dependence of the absorption coefficient in air ($T = 20°C$, $H = 70\%$ and $P = 1$ atm).

where f is the wave frequency in Hz, P is the atmospheric pressure in Pa ($P_{ref} = 101{,}325$ Pa), T is the absolute temperature in K ($T_{ref} = 293.15$ K), and f_{rO}, f_{rN} represent the relaxation frequencies of oxygen and nitrogen respectively, which also depend on temperature, pressure, and relative humidity. Fig. 1 represents the frequency dependence of this absorption coefficient, which has been generated from Eq. (2) assuming typical indoor values for the temperature ($T = T_{ref}$), pressure ($P = P_{ref}$), and humidity ($H = 70\%$). As can be seen, absorption increases very fast with frequency and it is above 0.5 dB/m in the ultrasonic region ($f > 20$ kHz), thus limiting the maximum range of these inaudible signals to some tens of meters in practice.

2.2 Propagation Speed

The speed of acoustic waves in air is an increasing function of temperature that can be approximated as,

$$c\,(\mathrm{m/s}) = 331.6 \cdot \sqrt{1 + \frac{T}{273.15}}, \tag{3}$$

where T represents temperature in Celsius. As can be easily inferred from Eq. (3), this speed is about six orders of magnitude lower than that of electromagnetic waves, what determines the high spatial resolution capability of this technology. On the negative side,

Doppler shift is a much more pronounced effect when using acoustic signals. Assuming a static receiver, the relative change of frequency caused by a moving emitter is given by,

$$\frac{\Delta f}{f_0} = \frac{v_e}{c}, \tag{4}$$

where $v_e \ll c$ is the emitter speed. From Eq. (4) it can be shown that the same shift caused in a radar signal by the fastest unmanned aerial vehicle ($v_e \approx 8000\,\text{m/s}$) is caused in an AAPS by a garden snail! ($v_e \approx 0.01\,\text{m/s}$).

2.3 Impedance

A third parameter that deserves some attention from AAPS designers is the specific acoustic impedance, which is a measure of the opposition that the medium presents to the acoustic flow, defined as,

$$Z_0\,(\text{rayls}) = \frac{p}{u}, \tag{5}$$

where p is the pressure at a certain point and u is the particle velocity at that point. Table 1 shows the acoustic impedance of air and typical building materials. Since the acoustic impedance of air is much lower than that of the building materials, acoustic waves propagating in air are almost perfectly reflected without phase change by those materials (reflection coefficient $R \approx 1$). Consequently, as opposed to radiofrequency-based positioning systems, signals generated by AAPS are confined within the room where the emitters have been deployed. This particularity also implies a strong multipath effect, as it is well known by acoustical engineers.

2.4 Outdoor Propagation

Most AAPS have been designed to operate indoors, with well controlled ambient conditions. However, these systems can be similarly deployed in outdoor environments if additional meteorological phenomena are considered.

To begin with, the atmospheric absorption represented in Eq. (2) can take a wider range of values because of the larger variability of temperature and humidity outdoors. Hence, this absorption could be more than five times greater during a hot and dry

Table 1 Specific Acoustic Impedance of Air and Typical Building Materials

Material	Z_0 (Rayls)
Air	413
Wood	1.57×10^6
Brick	7.40×10^6
Marble	10.5×10^6
Glass	13.0×10^6

summer evening than in a cold and humid winter morning. Also, additional attenuation phenomena such as the presence of fog or rain must be considered outdoors. A thick fog can be the main cause of attenuation for frequencies below 10 kHz (Cole and Dobbins, 1970; Davidson, 1975), and an intense rain can cause a nonnegligible attenuation for frequencies above 50 kHz (Shamanaeva, 1988).

Secondly, and due to the mechanical character of acoustic waves, wind modifies the apparent sound propagation speed as:

$$c\,(\mathrm{m/s}) = 331.6 \cdot \sqrt{1 + \frac{T}{273.15}} + v_l, \tag{6}$$

where v_l is the component of the wind parallel to the direction of propagation. In the atmosphere, both temperature and wind speed are functions of the altitude, and this dependence is inherited by the apparent propagation speed $c = c(z)$. This change of speed with altitude causes the refraction of acoustic waves, which in practice translates into a slight decrease in the received amplitude.

Atmospheric turbulence is the most problematic phenomenon when transmitting encoded acoustic signals outdoors, as it is a strongly random and nonlinear phenomenon. If an acoustic wave propagates through a turbulent medium, it finds a variety of strongly rotational fluxes (eddies) with different sizes, velocities, and temperatures. Each one of these eddies acts as a strong scatterer of acoustic energy and their combined effect alters the initial coherence of the wavefront, which will no longer be spherical and with identical amplitude after crossing the turbulent region. A receiver placed at a certain distance from the emitter will record random fluctuations in the amplitude and phase of the acquired signals. After a while, this effect can make the encoded signal completely unrecognizable by its matched receiver (Álvarez et al., 2006b).

3 Acoustic Signal Detection and Positioning Observables

As already mentioned in Section 1, one of the simplest methods to detect the arrival of an air-propagating acoustic pulse is the envelope detection technique represented in Fig. 2. This method rectifies and integrates the incoming signal, which is detected after exceeding a certain threshold. Envelope detection has been successfully used in many systems that do not require a very precise range measurement, as the popular Polaroid Ultrasonic Ranging System (Polaroid Corporation, 1991). Most of these systems incorporated an automatic control gain circuit in the receiver to compensate for the attenuation of ultrasound in air.

Once the received signal has been detected, there are different features of this signal that can be used for positioning purposes, commonly referred to as *positioning observables*,

- Power or Received Signal Strength (RSS), from where the traveled distance can be obtained if we know the emitted power and the attenuation model.

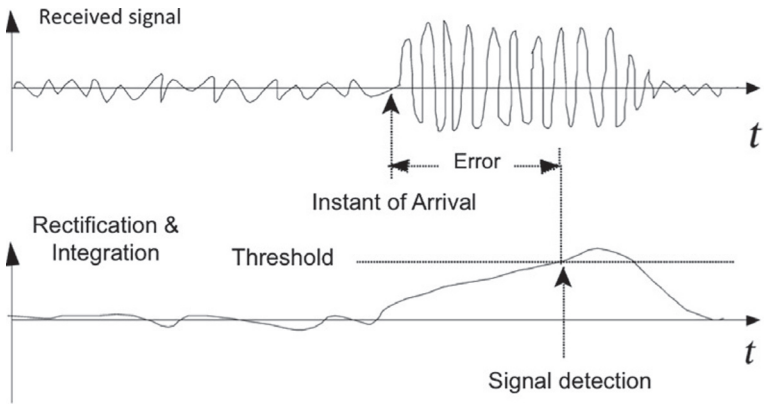

FIG. 2 Envelope detection technique.

- Time-of-Arrival (TOA), defined as the time at which the emitted signal reaches the receiver, from where the traveled distance can be easily obtained just by multiplying by the signal propagation speed.
- Time Difference of Arrival (TDOA), defined as the time difference between the moment the emitted signal is received and the moment a reference signal is received. As before, the difference in distances can be obtained by multiplying by the propagation speed.
- Angel of Arrival (AOA), from where the direction of the emitter can be inferred.

RSS is not commonly used in AAPS mainly due to nonuniform emission pattern of acoustic transducers and the strong dependence of air absorption with environmental parameters already described in Eq. (2). Besides, AOA is usually determined by measuring the different arrival times at an array of transducers. Hence, it can be stated that TOA and TDOA are the most common positioning observables when dealing with acoustic signals in air.

The precision of a time-delay measurement in an additive white Gaussian noise (AWGN) channel is given by (Kay, 1993)

$$\delta t \geq \frac{1}{\beta \cdot \sqrt{SNR}}, \tag{7}$$

where SNR is the signal-to-noise ratio at the output of the receiver and β is the effective or root mean square bandwidth. Eq. (7) states that to achieve a certain precision in a time-delay measurement a minimum value of the product bandwidth-SNR is required. Assuming a constant value for the SNR, this minimum bandwidth can be obtained by shortening the duration of the continuous frequency pulse, but then the amplitude of the signal should be increased to keep constant the signal energy. Actually, there is a physical limit for this amplitude imposed by both real transducers and electronics. An alternative is to modulate the original waveform to extend its bandwidth while keeping a constant energy, and use a matched filter in the receiver to detect this signal.

Two different alternatives have been proposed to modulate the emitted waveform with the aim of increasing its effective bandwidth. The first one is based on Linear Frequency Modulation (LFM), where the frequency of a pulsed waveform is linearly increased from f_1 to f_2 over the duration of the pulse. The second option is based on Binary Phase Coding, where a long pulse is divided into N subpulses whose phase is selected to be either 0 or π radians according to the bits of a certain code. If this code is a pseudo-random (PR) sequence, the waveform approximates a noise-modulated signal with a delta-like auto-correlation function. Fig. 3 shows a schematic representation of this broadband system. As can be seen, the TOA of the received signal is measured when the auto-correlation peak exceeds a certain threshold, thus improving the precision of the range measurement between one and two orders of magnitude with respect to that of narrowband systems. The main advantage of this approach is that different sequences from the same family can be generated with nearly null cross-correlation properties, thus allowing the simultaneous emission of different emitters with very low interference among them. To date, several broadband AAPS have been designed that propose the use of different families of PR sequences, such as Gold (Hazas and Ward, 2002), Kasami (Ureña et al., 2007), LS (Pérez et al., 2007), or CSS (Pérez et al., 2012). All these sequences exhibit very similar correlation properties, and the main difference between them is the possibility to design the matched filter shown in Fig. 3 as an efficient architecture that notably reduces the total number of arithmetic elements required to perform the correlations, thus allowing the actual implementation of a real-time operating system in a hardware platform. Examples of such efficient architectures in the receiver module of an airborne acoustic system can be found in Pérez et al. (2007, 2012) and Álvarez et al. (2006a)

4 Positioning Strategy

Two main positioning strategies have been developed in the design of AAPS, which are directly related to the main signal observables described in the previous section, namely, spherical and hyperbolic lateration. Although these techniques are not specific to acoustic

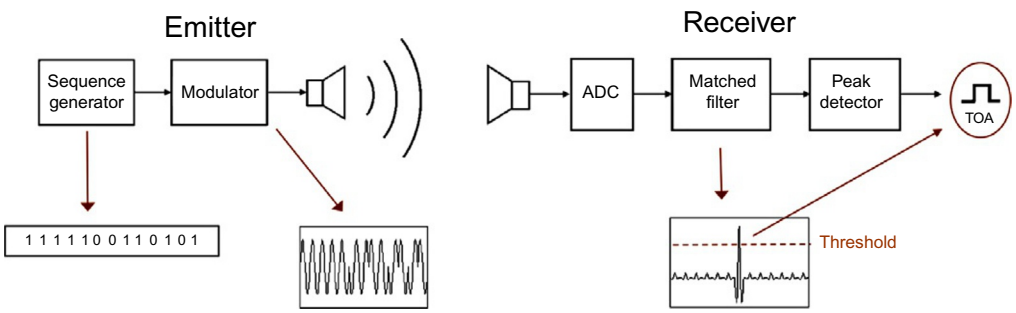

FIG. 3 Schematic representation of a broadband system based on Binary Phase Coding.

positioning systems, and detailed descriptions can be found elsewhere, they have been included in this chapter for completeness.

4.1 Spherical Lateration

Also known as trilateration, it can be defined as the method of determining the relative position of points by measuring absolute distances and using the geometry of spheres (see Fig. 4A). As mentioned before, absolute distance from the receiver to the *i*th beacon (d_i) can be easily obtained from the Time-of-Arrival of the signal emitted by this beacon (TOA_i) as,

$$d_i = c \cdot (TOA_i - t_{TX}), \tag{8}$$

where t_{TX} represents the instant of emission. Location is then obtained as the intersection of the spherical surfaces defined by these distances,

$$d_i = \sqrt{(x_i - x)^2 + (y_i - y)^2 + (z_i - z)^2}, \tag{9}$$

where (x_i, y_i, z_i) and (x, y, z) are the coordinates of the *i*th beacon and the receiver respectively. In three-dimensional geometry, a minimum of three TOAs (three beacons) are necessary to narrow the possible locations down to two, from which only one is usually

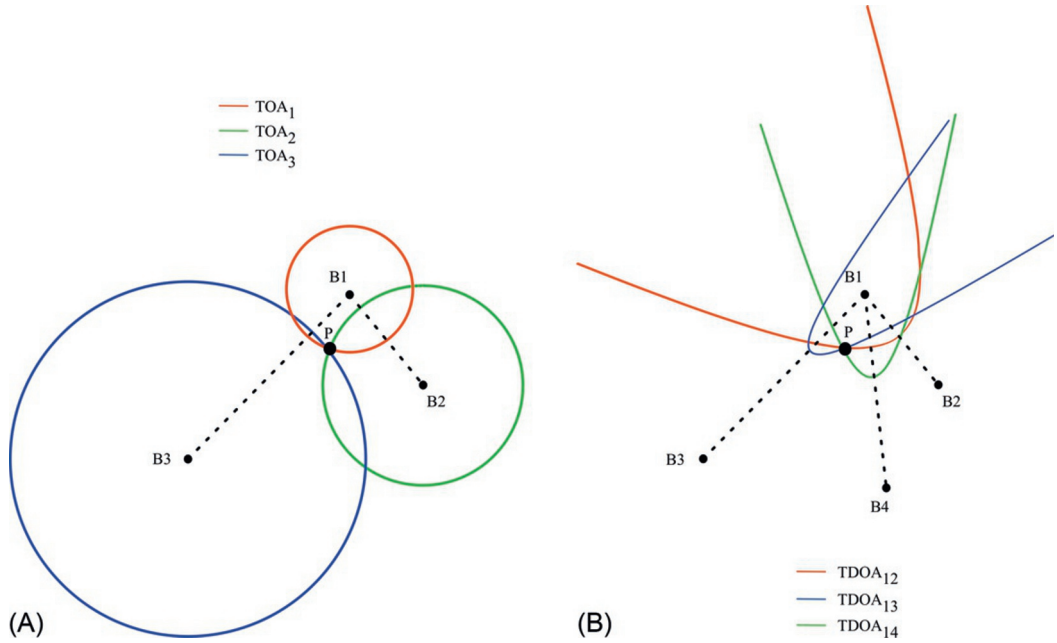

FIG. 4 Planar representation of the spherical (A) and hyperbolic (B) lateration techniques.

coherent with the geometry of the problem. Two families of methods are usually employed to solve the system of nonlinear equations represented in Eq. (9):

- Closed solution: the system is linearized by squaring the equations and introducing new variables. These methods are faster but less precise because the noise contribution is also squared. Besides, they require the participation of additional beacons to deal with the increased dimensionality of the problem. A representative example of this family is the Bancroft method (Bancroft, 1985).
- Iterative solution: equations are linearized by performing a Taylor expansion around an initial position estimate. The system is then iteratively solved to update the position until a final solution within a certain tolerance margin is obtained. These methods are slower than the previous ones and they also require an initial estimate, but in return they are more precise. A good example of this family is the Gauss-Newton algorithm (Bjorck, 1996).

The main inconvenient of spherical lateration is that the receiver must know the precise instant of emission (t_{TX}), and the emitters and receiver clocks must be synchronized, although this latter problem is not in acoustic systems as critical as it is in RF-based systems.

4.2 Hyperbolic Lateration

This strategy is also known as multilateration, and can be defined as the method of determining the relative position of points by measuring differential distances and using the geometry of hyperboloids (see Fig. 4B). This differential distance to the ith and jth beacons (d_{ij}) can be obtained from the time-difference-of-arrival of the signals emitted by them ($TDOA_{ij}$) as,

$$d_{ij} = c \cdot TDOA_{i,j}. \tag{10}$$

Location is in this case obtained as the intersection of the hyperbolic surfaces defined by these differential distances,

$$d_i - d_r = \sqrt{(x_i - x)^2 + (y_i - y)^2 + (z_i - z)^2} - \sqrt{(x_r - x)^2 + (y_r - y)^2 + (z_r - z)^2}, \tag{11}$$

where (x_i, y_i, z_i), (x_r, y_r, z_r), and (x, y, z) are the coordinates of the ith beacon, the reference beacon, and the receiver respectively. In three-dimensional geometry, a minimum of three TDOAs (four beacons) are necessary to narrow the possible locations down to 2 (again from which only one is usually coherent). The same methods employed to solve the set of spherical lateration equations can be used to solve the set of hyperbolic lateration equations. Note that in this positioning strategy only the emitters must be synchronized between them, but not with the receiver.

More beacons than the minimum required in each case can be used to introduce redundancy, thus obtaining an overdetermined system of equations. In this case, the system can be solved as a least squares problem.

5 Detection Hindering Phenomena and Compensation Strategies

The use of simultaneous and encoded emissions described at the end of Section 3, which notably improves the precision of the range measurements and robustness to in-band noise of broadband AAPS, comes hand-in-hand with new problems that may hinder the detection of these signals. Most recent research in the field of AAPS is partially devoted to the development of compensation algorithms for these phenomena. The most relevant are briefly described next.

5.1 Multiple Access Interference

The signal $r(t)$ received in a broadband AAPS, with N beacons simultaneously emitting binary phased coded signals $g_j(t)$ is given by,

$$r(t) = \sum_{j=1}^{N} A_j \cdot (h_j * g_j)(t - t_j) + n(t), \tag{12}$$

where t_j and A_j are respectively the TOA and amplitude of the signal to be estimated, and $n(t)$ represents the channel additive noise. The effect on the signal $g_j(t)$ of the acoustic channel is introduced by the convolution term $h_j(t)$, which represents the a priori unknown channel impulse response. As mentioned before, the output of the receiver is formed by correlation of $r(t)$ with all the signal patterns. For the kth beacon we have,

$$R_{rg_k}(t) = A_k \cdot (h_k * R_{g_k g_k})(t - t_k) + \sum_{j \neq k} A_j \cdot (h_j * R_{g_k g_j})(t - t_j) + \eta(t), \tag{13}$$

where $R_{g_k g_j}(t)$ represents the cross-correlation of codes $g_k(t)$ and $g_j(t)$ and $\eta(t)$ is the convolved noise. As Eq. (13) indicates, there are two effects which deteriorate the estimation of the TOAs: Intersymbol Interference (ISI), which is due to the fact that the limited bandwidth of the acoustic channel lowers the correlation peaks and degrades the signal detection and ranging; and Multiple-Access Interference (MAI) among all the emitted codes in which larger amplitude signals make difficult the detection of weaker signals emitted simultaneously. Combined, both effects can lead to large deviations of the TOAs estimates from their true values. This effect can be compensated by using recursive subtractive techniques, such as the Parallel Interference Cancelation algorithm (Aguilera et al., 2018b), but at the expense of increasing the time required to compute a new position estimate. It could also be attenuated by recovering the time-multiplexing strategy used in

narrowband systems but with encoded emissions that can help identify the corresponding emitter, as proposed in Álvarez et al. (2017b).

5.2 Strong Multipath Propagation

As we have already stated in Section 2.3, multipath propagation is a common effect in indoor AAPS due to the specular reflections of the acoustic emissions at the room boundaries. This phenomenon gives rise to typical room impulse responses where the direct path is followed by a pattern of early reflections and then by a late-field reverberant tail, as the one shown in Fig. 5A. Since the pattern of early reflections is basically the representation of a sparse channel whose number of coefficients with nonnegligible magnitude is much lower than the total number of coefficients (see Fig. 5B), a matching pursuit (MP) algorithm can be used as a low complexity approximation to the maximum likelihood solution to estimate the TOA of the direct wave (Kim and Iltis, 2004).

If we consider N different beacons, the digitized samples of the received signal $\mathbf{r}$ can be represented by,

$$\mathbf{r} = \sum_{l=1}^{N} \mathbf{E}^l \mathbf{h}^l + \mathbf{n}, \tag{14}$$

where $\mathbf{h}^l$ is the lth channel coefficient vector, $\mathbf{E}^l$ is the characteristic signal matrix containing samples of the lth beacon emission, and $\mathbf{n}$ is a vector of zero-mean white Gaussian

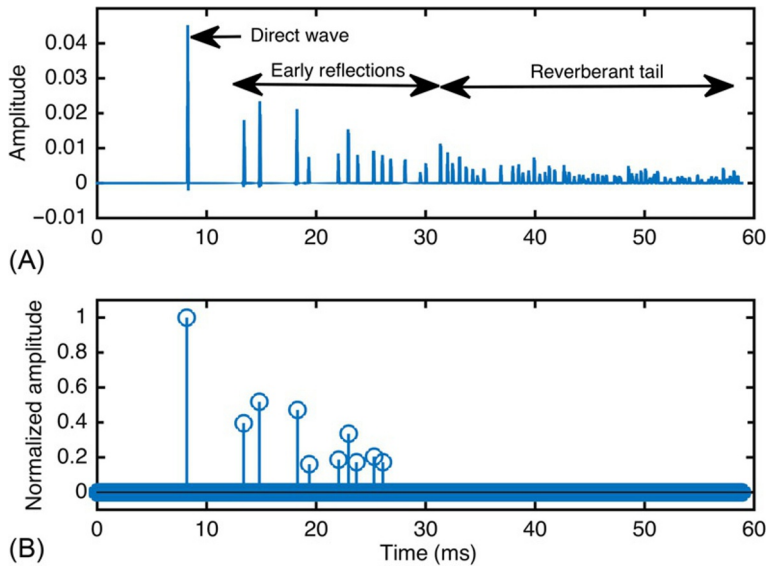

FIG. 5 (A) Acoustic impulse response of a room with highly reflective walls and (B) equivalent 10-coefficient sparse channel model.

noise samples. The MP algorithm estimates the channel coefficients $\hat{h}^l_{q_j}$ one at a time, using a greedy approach in which the detected path index q^l_j and corresponding coefficient $\hat{h}^l_{q_j}$ are computed from the following set of equations,

$$q^l_j = \underset{i \neq q^l_1, \ldots, q^l_{j-1}}{\operatorname{argmax}} \left\{ \frac{\left| (\mathbf{E}^l_i)^H \mathbf{r}^j \right|^2}{\left\| \mathbf{E}^l_i \right\|^2} \right\}, \tag{15}$$

and

$$\hat{h}^l_{q_j} = \frac{(\mathbf{E}^l_{q_j})^H \mathbf{r}^j}{\left\| \mathbf{E}^l_{q_j} \right\|^2}, \tag{16}$$

with

$$\mathbf{r}^{j+1} = \mathbf{r}^j - \frac{(\mathbf{E}^l_{q_j})^H \mathbf{r}^j \mathbf{E}^l_{q_j}}{\left\| \mathbf{E}^l_{q_j} \right\|^2}, \tag{17}$$

where $\mathbf{E}^l_i$ represents the ith column vector of matrix $\mathbf{E}^l$ and $\mathbf{r}^1 = \mathbf{r}$. Every new iteration of the algorithm $j = 1, 2, \ldots, N_f$, computes Eqs. (15) and (16) N times (one per channel), and only the largest coefficient $\hat{h}^l_{q_j}$ is stored. Next, the newly estimated signal $\hat{h}^l_{q_j} \mathbf{E}^l_{q_j}$ is subtracted from the current residue $\mathbf{r}^j$ to obtain the updated signal $\mathbf{r}^{j+1}$ as indicated by Eq. (17). This multipath cancelation technique has proven to notably decrease the mean positioning error measured under strong multipath conditions in an AAPS where a 16 kHz sonic carrier was modulated with 63-bit Kasami sequences (Álvarez et al., 2017a), and an AAPS based on a time-multiplexing strategy where a 41.67 kHz ultrasonic carrier was modulated with 255-bit Kasami sequences (Aguilera et al., 2018a).

5.3 Doppler Shift

In Section 2.2 we have seen that the low speed of sound in air responsible for the relatively high resolution of AAPS is also the cause of a strong Doppler shift. This phenomenon has no effect on envelope detection receivers, but can make broadband signals completely unrecognizable to the matched receiver. A straightforward solution to this problem would be to replace the single correlator at the receiver for a bank of them, each one matched to different frequency-shifted versions of the code to be detected. However, this simple implementation would require a very high operation frequency at the receiver if a fine Doppler resolution is required.

An alternative approach consists in using a multirate filter bank to compensate for the Doppler shift caused by the receiver's movement, following the scheme shown in Fig. 6. Let assume that the received signal $r(t)$ is sampled at f_s, thus giving the discrete-time signal $r[n]$ with spectrum $R(e^{j\omega})$. This signal is first expanded by a factor Q by including $Q - 1$ zeroes between consecutive samples of $r[n]$. A new signal $r_i[n] = r[n/Q]$ for

$n = 0, \pm Q, \pm 2Q, \ldots$ and 0 otherwise, is thus obtained whose spectrum $R_i(e^{j\omega})$ is a Q-fold compressed version of $R(e^{j\omega})$, i.e.,

$$R_i(e^{j\omega}) = R(e^{j\omega Q}). \tag{18}$$

As shown in Fig. 6, the expanded signal $r_i[n]$ is next filtered by a low-pass (LP) filter whose transfer function is given by,

$$H_{LP}(e^{j\omega}) = \begin{cases} Q & 0 \le |\omega| \le \pi/Q \\ 0 & \text{otherwise} \end{cases} \tag{19}$$

to obtain a new signal $r_f[n]$ with spectrum $R_f(e^{j\omega})$ given by,

$$R_f(e^{j\omega}) = \begin{cases} Q \cdot R(e^{j\omega Q}) & 0 \le |\omega| \le \pi/Q \\ 0 & \text{otherwise.} \end{cases} \tag{20}$$

This signal is then fed into a bank of K decimators with decimation factor of $Q - k + (K+1)/2$, for $k = [1, 2, \ldots, K]$, from where K signals $r_{d,k}[n] = r_f[n \cdot (Q - k + (K+1)/2)]$ are obtained. Assuming the absence of aliasing, the spectra $R_{d,k}(e^{j\omega})$ of these signals are given by,

$$R_{d,k}(e^{j\omega}) = \frac{Q}{Q - k + (K+1)/2} R(e^{j\omega \frac{Q}{Q+(K+1)/2-k}}), \quad 0 \le |\omega| \le \pi, \quad k = [1, 2, \ldots, K]. \tag{21}$$

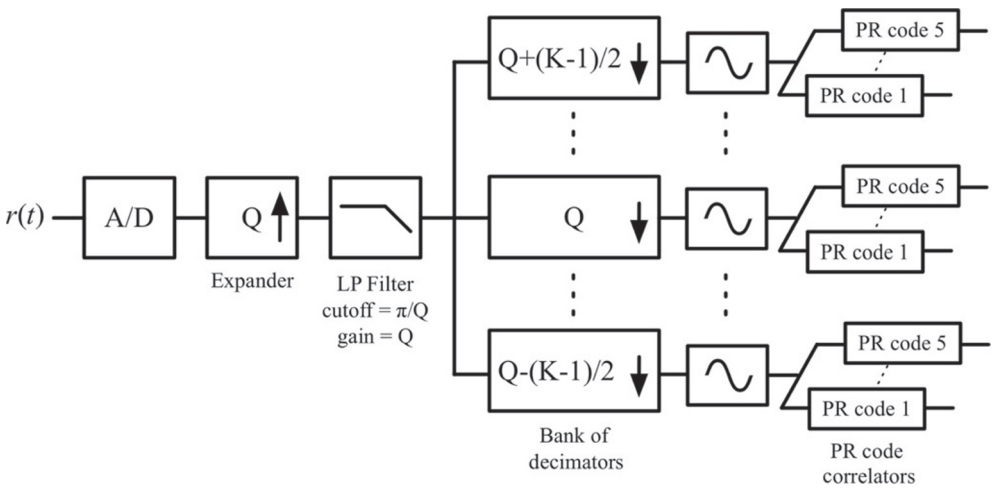

FIG. 6 Block diagram of the Doppler-tolerant receiver based on a multirate filter bank.

If the received signal $r(t)$ has been emitted as the pattern $p(t)$ by a certain beacon, and the receiver is moving toward this beacon with speed v_{r_k}, the spectra of the discrete-time versions of these signals $r[n]$ and $p[n]$ are related as,

$$R(e^{j\omega}) = P\left(e^{j\omega\frac{c}{c+v_{r_k}}}\right), \tag{22}$$

where c is again the speed of sound. Combining Eqs. (21) and (22) the spectra of the signals coming out from the decimators can be finally expressed as,

$$R_{d,k}(e^{j\omega}) \propto R\left(e^{j\omega\frac{Q}{Q+(K+1)/2-k}}\right) = P\left(e^{j\omega\frac{Q}{Q+(K+1)/2-k}\frac{c}{c+v_{r_k}}}\right). \tag{23}$$

From this latter expression, it is clear that the frequency shift caused by the receiver's movement is canceled if,

$$\frac{Q}{Q+(K+1)/2-k}\frac{c}{c+v_{r_k}} = 1. \tag{24}$$

Assuming $|v_{r_k}| \ll c$, the factor Q can be obtained from Eq. (24) as,

$$Q \approx \left(k - \frac{K+1}{2}\right)\frac{c}{v_{r_k}}. \tag{25}$$

This Doppler tolerant receiver was used in Álvarez et al. (2013) to improve the detection rate of broadband signals (40 kHz carrier modulated with 255-Kasami sequences), which were acquired by the receiver when moving in a horizontal plane with linear velocities of up to 6.82 m/s.

A different solution to compensate for this phenomenon consists in using intrinsically Doppler resilient polyphase codes to modulate the emissions of the AAPS. Although some works have already explored this interesting alternative (Paredes et al., 2011), their experimental results are limited by the bandwidth constraints of current acoustic transducer.

6 Conclusions

This chapter has presented the fundamentals of airborne acoustic positioning systems. First, the main phenomena affecting the propagation of acoustic waves in air have been reviewed to explain some specific features of this technology, such as high precision (centimeter), limited coverage (tens of meters), and room confined emissions. Also, additional phenomena that should be considered outdoors have been briefly described.

The most important positioning observables, namely, Time-of-Arrival (TOA) and Time-Difference-Of-Arrival (TDOA) have been then presented together with different methods to detect the arrival of acoustic signals. It has been seen that Binary Phase Coding can be used to extend the bandwidth of the emitted signals and improve the precision of the range measurements, at the expense of increasing the complexity of the receiver. In the last years, an important effort in this field of research has been devoted to the proposal of better encoding schemes and the design of the corresponding efficient correlation architectures. The positioning strategies directly related to these observables have been reviewed next, placing the emphasis on the different methods usually employed to solve the spherical and hyperbolic system of equations derived from the TOA and TDOA measurements respectively.

Finally, three different detection hindering phenomena and some of the strategies developed to compensate them, have been included in the last section of this chapter to provide the reader an insight into the most recent research in this active field of research.

References

Aguilera, T., Álvarez, FJ., Gualda, D., Villadangos, J.M., Herněndez, A., Ureña, J.U., 2018a. Multipath compensation algorithm for TDMA-based ultrasonic local positioning systems. IEEE Trans. Instrum. Meas. 67 (5), 984–991.

Aguilera, T., Seco, F., Álvarez, FJ., Jiménez, A., 2018b. Broadband acoustic local positioning system for mobile devices with multiple access interference cancellation. Measurement 116, 483–494.

Álvarez, FJ., Hernández, A., Ureña, J.U., Mazo, M., García, J.J., Jiménez, J.A., Jiménez, A., 2006a. Real-time implementation of an efficient correlator for complementary sets of four sequences applied to ultrasonic pulse compression systems. Microprocess. Microsyst. 30, 43–51.

Álvarez, FJ., Urena, J., Mazo, M., Hernandez, A., Garcia, J.J., Marziani, C.D., 2006b. High reliability outdoor sonar prototype based on efficient signal coding. IEEE Trans. Ultrason. Ferroelectr. Freq. Control 53 (10), 1862–1871.

Álvarez, FJ., Hernández, A., Moreno, J.A., Pérez, M.C., Ureña, J.U., Marziani, C.D., 2013. Doppler-tolerant receiver for an ultrasonic LPS based on Kasami sequences. Sens. Actuators A: Phys. 189 (Supplement C), 238–253.

Álvarez, FJ., Aguilera, T., López-Valcarce, R., 2017a. CDMA-based acoustic local positioning system for portable devices with multipath cancellation. Digital Signal Process. 62 (Suppl. C), 38–51.

Álvarez, FJ., Esteban, J., Villadangos, J.M., 2017b. High accuracy APS for unmanned aerial vehicles. In: 13th International Conference on Advanced Technologies, Systems and Services in Telecommunications, Nis, Serbia, pp. 1–6.

Bancroft, S., 1985. An algebraic solution to the GPS equations. IEEE Trans. Aerosp. Electron. Syst. AES-21 (7), 56–59.

Bjorck, A., 1996. Numerical Methods for Least Squares Problems. SIAM.

Cole, J.E., Dobbins, R.A., 1970. Propagation of sound through atmospheric fog. J. Atmos. Sci. 27 (3), 426–434.

Davidson, G.A., 1975. Sound propagation in fogs. J. Atmos. Sci. 32 (11), 2201–2205.

Foxlin, E., Harrington, M., 1998. Constellation: A Wide-Range Wireless Motion-Tracking System for Augmented Reality and Virtual Set Applications. ACM Press.

Hazas, M., Ward, A., 2002. A Novel Broadband Ultrasonic Location System. In: UbiComp 2002: Ubiquitous Computing: 4th International Conference Göteborg, Sweden, September 29–October 1, 2002 Proceedings, pp. 264–280.

Hazas, M., Ward, A., 2003. A high performance privacy-oriented location system. In: Proceedings of the First IEEE International Conference on Pervasive Computing and Communications, 2003 (PerCom 2003), pp. 216–223.

ISO/TC 43 Technical Committee, Acoustics, Sub-Committee SC1, Noise, 1993. Attenuation of sound during propagation outdoors. Part 1: Calculation of the absorption of sound by the atmosphere. Tech. Rep. ISO 9613-1:1993(E). International Organization for Standardization, Geneve, Switzerland.

Jörg, K.-W., Berg, M., 1998. Sophisticated mobile robot sonar sensing with pseudo-random codes. Robot. Auton. Syst. 25 (3), 241–251.

Kay, S.M., 1993. Fundamentals of Statistical Signal Processing: Estimation Theory (Signal Processing Series). Englewood Cliffs, NJ, USA: Prentice-Hall.

Kim, S., Iltis, R.A., 2004. A matching-pursuit/GSIC-based algorithm for DS-CDMA sparse-channel estimation. IEEE Signal Process. Lett. 11 (1), 12–15.

Mautz, R., 2012. Indoor positioning technologies. Ph.D. thesis, Institute of Geodesy and Photogrammetry, Department of Civil, Environmental and Geomatic Engineering, ETH Zurich.

Milne, P.H., 1983. Underwater Acoustic Positioning Systems. Gulf Publishing Company, Houston, TX.

Paredes, J.A., Aguilera, T., Álvarez, F.J., Lozano, J., Morera, J., 2011. Analysis of Doppler effect on the pulse compression of different codes emitted by an ultrasonic LPS. Sensors 11, 10765–10784.

Peremans, H., Audenaert, K., Campenhout, J.M.V., 1993. A high-resolution sensor based on tri-aural perception. IEEE Trans. Robot. Autom. 9 (1), 36–48.

Pérez, M.C., Ureña, J.U., Hernández, A., de Marziani, C., Jimenez, A., Villadangos, J.M., Álvarez, F.J., 2007. Ultrasonic beacon-based local positioning system using loosely synchronous codes. In: 2007 IEEE International Symposium on Intelligent Signal Processing, pp. 1–6.

Pérez, M.C., Serrano, R.S., Ureña, J.U., Hernández, A., Marziani, C.D., Álvarez, F.J., 2012. Correlator implementation for orthogonal CSS used in an ultrasonic LPS. IEEE Sens. J. 12 (9), 2807–2816.

Polaroid Corporation, 1991. Ultrasonic Ranging Systems.

Priyantha, N.B., Chakraborty, A., Balakrishnan, H., 2000. The cricket location-support system. In: Proceedings of the 6th Annual International Conference on Mobile Computing and Networking, MobiCom '00. ACM, New York, pp. 32–43.

Shamanaeva, L.G., 1988. Acoustic sounding of rain intensity. J. Acoust. Soc. Am. 84 (2), 713–718.

Skolnik, M.I., 1980. Introduction to Radar Systems, second ed. McGraw Hill Book Co., New York.

Ureña, J.U., Mazo, M., García, J.J., Hernández, A., Bueno, E., 1999. Classification of reflectors with an ultrasonic sensor for mobile robot applications. Robot. Auton. Syst. 29 (4), 269–279.

Ureña, J.U., Hernández, A., Jiménez, A., Villadangos, J.M., Mazo, M., García, J.C., García, J.J., Álvarez, F.J., de Marziani, C., Pérez, M.C., Jiménez, J.A., Jiménez, A.R., Seco, F., 2007. Advanced sensorial system for an acoustic LPS. Microprocess. Microsyst. 31 (6), 393–401.

Villadangos, J.M., Urena, J., Mazo, M., Hernandez, A., Alvarez, F.J., Garcia, J.J., Marziani, C.D., Alonso, D., 2005. Improvement of ultrasonic beacon-based local position system using multi-access techniques. In: IEEE International Workshop on Intelligent Signal Processing, 2005, pp. 352–357.

Ward, A., Jones, A., Hopper, A., 1997. A new location technique for the active office. IEEE Pers. Commun. 4 (5), 42–47.